npj | 2D Materials and Applications

www.nature.com/npj2dmaterials

ARTICLE OPEN

Check for updates

A swift technique to hydrophobize graphene and increase its mechanical stability and charge carrier density

Lukas Madauß[1], Erik Pollmann[1], Tobias Foller[2], Jens Schumacher[3], Ulrich Hagemann[4], Tobias Heckhoff[1], Matthias Herder[1], Lucia Skopinski[1], Lars Breuer[1], Anke Hierzenberger[1], Alexandra Wittmar[3], Henning Lebius[5], Abdenacer Benyagoub[5], Mathias Ulbricht[3], Rakesh Joshi[2] and Marika Schleberger[1]✉

Despite the improvement of the quality of CVD grown single-layer graphene on copper substrates, transferring the two-dimensional layer without introducing any unintentional defects still poses a challenge. While many approaches focus on optimizing the transfer itself or on necessary post-transfer cleaning steps, we have focused on developing a pre-treatment of the monolayer graphene on copper to improve the quality and reproducibility of the transfer process. By pressing an ethylene-vinyl acetate copolymer foil onto the monolayer graphene on copper using a commercially available vacuum bag sealer graphene is stabilized by the attachment of functional carbon groups. As a result, we are able to transfer graphene without the need of any supporting layer in an all-H_2O wet-chemical transfer step. Despite the general belief that the crumbling of graphene without a support layer in a H_2O environment is caused due to differences in surface energy, we will show that this assumption is false and that this behavior is caused rather by the polar interactions between graphene and water. Suppressing these interactions protects graphene from ripping and results in extremely clean, highly crystalline graphene with a coverage close to 100%.

npj 2D Materials and Applications (2020)4:11 ; https://doi.org/10.1038/s41699-020-0148-9

INTRODUCTION

Despite intensive research in graphene since its discovery in 2004, the interest in the two-dimensional (2D) material is still growing[1–5]. Owing to its exceptional electrical and mechanical properties, its applicability as a membrane or pressure sensor, graphene remains a highly investigated material[6–15]. While initial experiments were mainly performed with exfoliated graphene flakes, the drawbacks of this approach such as low reproducibility and small flake sizes have shifted the focus towards complementary synthesis procedures. In particular, the precondition for every graphene-based industrial application is the feasibility of up-scaling. Driven by this aim, researchers have started focusing on the growth of graphene (Gr) via chemical vapor deposition (CVD). Even though efforts are made towards the direct growth of graphene onto any desired material, copper (Cu) still remains the most used material for CVD growth of graphene[16–21]. However, most applications require the transfer of the 2D layer onto another substrate—a process still posing a challenge. While nearly all transfer techniques discussed in literature focus on optimizing the actual transfer step, we will present a pre-treatment technique of the Gr/Cu, which allows us to perform a polymer-free, wet-chemical transfer of the graphene in an all-H_2O environment[22–27]. Inspired by the work on reduced graphene oxide (rGO) membranes aiming for homogeneous evenly spaced rGO laminates, we apply a fast and straightforward approach to decorate the graphene with stabilizing functional carbon groups, which strongly increase the stability of our graphene sheet during transfer hence making all polymer-based sacrificial layer redundant.

RESULTS

Surface modifications of graphene

The common transfer method of CVD grown graphene from a Cu surface onto another substrate involves a polymer supporting layer on top of the graphene, e.g., poly(methyl methacrylate) (PMMA), polyvinyl alcohol (PVA), or paraffin acting as a stabilizer and preventing graphene from ripping during the transfer[28–31]. Dissolving the polymer after the transfer however frequently causes many problems mainly due to polymer residues on the graphene surface, which drastically alter and degrade graphene´s properties[32–34]. So far, every reported transfer or cleaning technique of CVD graphene in order to avoid or remove the polymer support afterwards involves additional chemicals, long-time heating processes or is restricted to certain target materials[30,35,36].

In contrast, our pre-treatment of the Gr/Cu involves a flattening step using a commercially available vacuum bag sealing machine with ethylene-vinyl acetate copolymer (EVAC) as the bag material, see Fig. 1 (Supplementary Fig. 1 gives additional characterization information on the bag material). Having flattened the complete Gr/Cu sample, we can place the Gr/Cu on an ammonium persulfate (APS) solution. After etching off the Cu and gradually diluting the APS solution with H_2O, a target substrate can be used to scoop out the graphene sheet. Note that the final transfer is performed in a pure H_2O environment where no supporting layer for stabilization is necessary once the flattening step had been applied. The effect of the flattening already becomes visible when looking at the non-supported graphene layer floating on the APS etching solution, shown in Fig. 2a. While the flattened graphene maintains its rectangular form determined by the shape of the initial Gr/Cu wafer, the non-treated graphene crumbles and rips. The same results are obtained once the graphene sheets have

[1]University of Duisburg-Essen, Faculty of Physics and CENIDE, 47057 Duisburg, Germany. [2]University of New South Wales, School of Materials Science and Engineering, Kensington, NSW 2052, Australia. [3]University of Duisburg-Essen, Technical Chemistry II and CENIDE, 45117 Essen, Germany. [4]University of Duisburg-Essen, CENIDE, ICAN, 47057 Duisburg, Germany. [5]Normandie Univ, ENSICAEN, UNICAEN, CEA, CNRS, CIMAP, 14000 Caen, France. ✉email: marika.schleberger@uni-due.de

Published in partnership with FCT NOVA with the support of E-MRS

npj nature partner journals

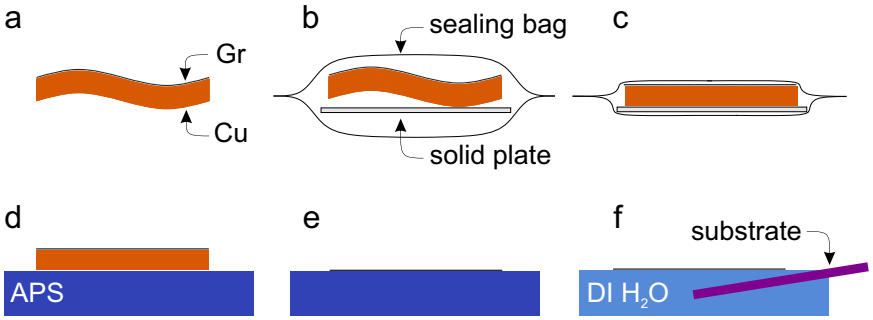

Fig. 1 Process steps of flattening Gr/Cu using an ethylene-vinyl acetate copolymer foil. a–c Flattening of Gr/Cu is achieved by using a vacuum bag sealing machine. **d–f** An aqueous ammonium persulfate solution is used for etching the Cu. After diluting with DI H_2O, graphene can be scooped out with the target substrate.

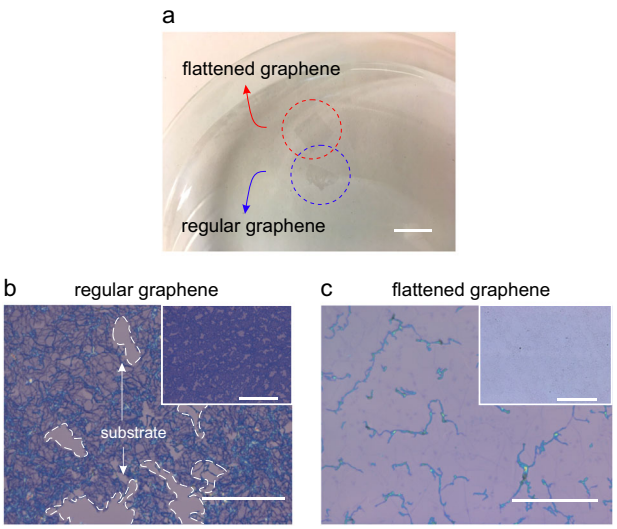

Fig. 2 Optical images of regular and pre-treated graphene during and after transfer. a Flattened and regular graphene floating on an APS etching solution. Scale bar is 1 cm. **b**, **c** Optical microscopy images of non-flattened and flattened graphene transferred onto Si/SiO_2 substrates. Scale bars are 40 µm for main images and 500 µm for insets, respectively.

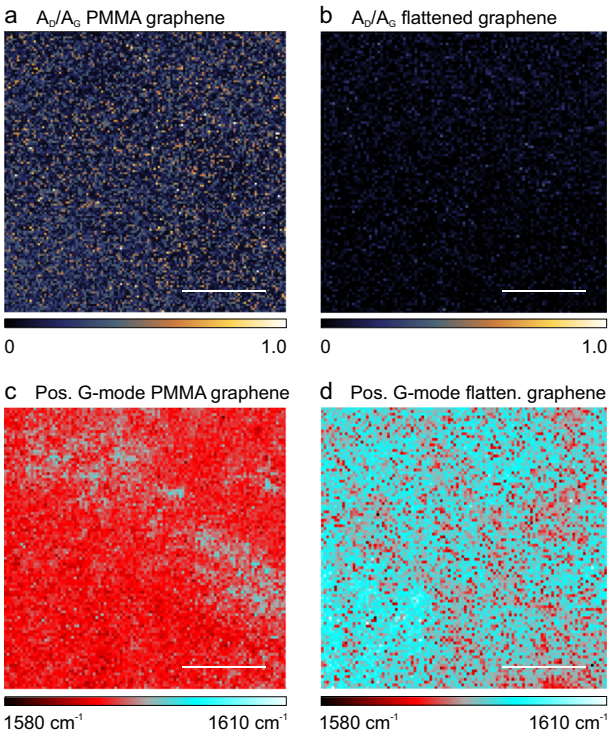

Fig. 3 Raman spectroscopy maping of graphene transferred with and without PMMA. Intensity ratios of D- and G-mode of **a** PMMA-transferred and **b** flattened graphene. Raman shift of graphene's G-mode is presented in **c** and **d** for PMMA-transferred and flattened graphene, respectively. Neither of the samples had been treated by any means after the transfer. After scooping graphene out of the H_2O with a SiO_2/Si wafer, the samples were left to dry under ambient conditions. Scale bars for **a–d** are 500 µm.

been transferred, see Fig. 2b for regular graphene and Fig. 2c for flattened graphene, respectively. The latter one shows a perfectly homogeneous coverage over the whole sample. The non-processed graphene, however, not only displays tens of µm^2-sized uncovered regions, but even the covered parts show poor smoothness and countless wrinkles.

In order to evaluate the success of the transfer method presented here in terms of quality and coverage, we will compare the pre-flattened graphene with conventionally transferred graphene supported by a PMMA layer (in the following referred to as PMMA graphene) after transfer onto a SiO_2 substrate. For this, we have performed Raman mappings. By plotting the intensity ratio of graphene´s Raman active defect(D)-mode and graphite(G)-mode, we can visualize the density of defects in graphene. Raman measurements indeed confirm an extremely low-defect density with an average A_D/A_G intensity ratio of ~0.04 for the flattened graphene compared to an intensity ratio of ~0.2 for the PMMA-assisted graphene transfer as shown in Fig. 3a, b (note that neither of the samples have undergone any additional ethanol rinsing, heat treatment or similar). Supplementary Fig. 2 presents representative Raman spectra of graphene for both transfer techniques. Aside from a highly crystalline graphene layer, we observe a considerably high charge-carrier density in graphene induced by charge transfer as can be derived from the peak position of the G-mode in the Raman mappings, see Fig. 3c, d for PMMA-transferred graphene and flattened graphene, respectively. Even though PMMA is known as a strong p-dopant for graphene, the flattened graphene displays an even higher level of doping, most likely originating from the two oxygen atoms present in the side group (acetate) which will promote a charge transfer due to oxygen's strong electronegativity and presumably facilitated by the intimate contact at the interface between the rubbery EVAC and graphene and the weaker bond (C–O) between polymer main chain and side group (acetate), compared to glassy PMMA with a C–C bond to the side group (methyl ester); see also the mass spectroscopy results of surface analysis below. Comparing the Raman shift of the G-mode (and I_{2D}/I_G intensity ratio, see Supplementary Fig. 3) of the flattened graphene with the work

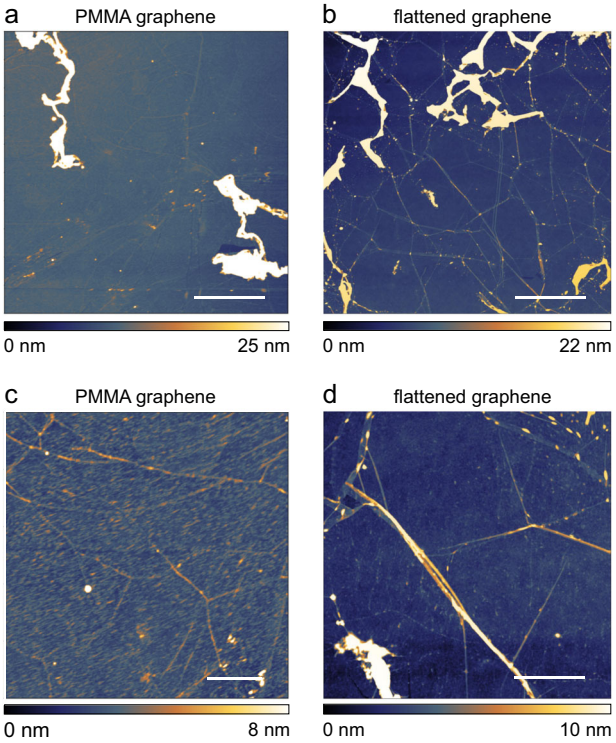

Fig. 4 AFM images of graphene transferred with and without PMMA. AFM images of transferred CVD graphene onto SiO_2 substrates with **a**, **c** and without **b**, **d** PMMA support. Graphene supported with PMMA during the transfer shows high density of nm-sized polymer residues after dissolving the PMMA layer, whereas the flattened graphene is nearly free of any contaminations. Note the different scale bars in **c** and **d**, underlining the huge improvement in cleanliness. The bright spots in **b** and **d** are no polymer residues from the flattening foil but overlapping graphene parts or wrinkles resulting from the drying process after scooping out graphene with a target wafer. Scale bar is 5 μm for **a**, **b**, 1 μm for **c**, and 2.5 μm for **d**.

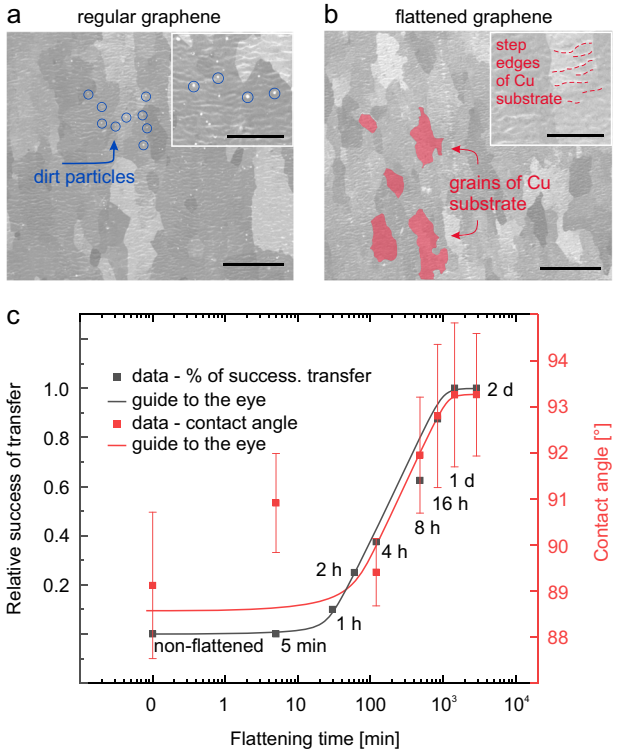

Fig. 5 SEM images of regular and flattened Gr/Cu as well as analysis of transfer success rate and Gr/Cu–water contact angle as a function of flattening time. SEM images of **a** regular and **b** flattened Gr/Cu. Scale bars are 250 μm for main images and 100 μm for insets. **c** Dependency of the relative success of transfer and contact angle on flattening time of Gr/Cu. Error bars represent standard deviations.

of Bruna et al.[37], we can conclude that both transferred samples exhibit a p-doped behavior with a charge carrier concentration of $\sim 5 \times 10^{12}$ cm^{-2} for the PMMA-transferred and 1.5×10^{13} cm^{-2} for the flattened graphene[37]. The combination of an extremely low-defect density and a high level of charge carriers in graphene is expected to be beneficial for a high charge-carrier mobility. The flattening step thus proves to be an effective and gentle way for doping graphene.

In addition to an extremely low-defect density, another advantage of a polymer-free transfer is the avoidance of persistent polymer residues on the graphene surface after dissolving the support layer. Numerous cleaning procedures of polymer contaminated graphene have been presented in literature. However, despite time-consuming cleaning steps, polymer residues are almost impossible to remove completely. This in turn causes a downgraded electrical performance of graphene, an uncontrollable and inhomogeneous doping level or makes it simply useless for atomic force microscopy (AFM), and in particular transmission electron microscopy (TEM) measurements, which typically demand a high degree of cleanliness[32,34,35,38,39]. Figure 4 presents AFM measurements of graphene transferred with (a, c) and without (b, d) PMMA support. While Fig. 4a, c display numerous nanometer sized PMMA leftovers, we obtain large areas of perfectly clean graphene surface for flattened graphene in Fig. 4b, d.

Let us now address the reason for the enhanced mechanical stability and improved quality of the graphene once it has been modified by our approach. Arguing that the copper itself has been flattened on a microscopic scale, hence providing a more uniform and smoother surface for the graphene is highly unlikely. SEM images shown in Fig. 5a, b of regular and flattened CVD graphene on Cu, respectively, reveal no observable differences in terms of the smoothness of the Cu substrate (aside from a reduced dirt particle density for the flattened Gr/Cu). It is much more plausible that the very surface of graphene itself has been altered by our approach. In order to draw conclusions about the flattening step, the success rate in transfer, and the flattening time, we studied how graphene behaves during the transfer when varying the flattening time, the result of which is presented in Fig. 5c. We found that there is a clear dependency of the transfer success rate (corresponding to graphene not ripping/crumbling) and the flattening time. While we were practically never able to successfully transfer non-flattened graphene, we obtained a success rate of 100% after just one day of flattening. Relating this observation with the change of the contact angle of a water droplet on the Gr/Cu surface, also shown in Fig. 5c, we can draw two important conclusions: (i) both the transfer success rate and the contact angle have their lowest values for non-treated Gr/Cu with values of 0 and 89.1°, respectively. After 1 day of flattening, the success rate and the contact angle have increased displaying values of 1 and 93.1°. (ii) Neither of the two values change when we further increase the flattening time indicating that the responsible mechanism during the flattening step has converged. Since a large contact angle between a water droplet and a surface typically indicates hydrophobic properties of the surface, we can conclude that the flattening increases the hydrophobicity of the graphene. A saturation of the contact angle most likely results from the fact that once the majority of graphene's surface has been decorated with adsorbates, additional molecules are less

likely to attach to graphene as nearly all free adsorption sites have already been filled. Even if additional layers of adsorbates would remain on graphene's surface, the contact angle is not expected to change any more as it is predominantly governed by the layers in direct contact.

DISCUSSION

To further address this observation, we performed X-ray photoelectron spectroscopy (XPS) measurements to confirm the presence of additional adsorbates on graphene's surface. Owing to the surface sensitivity of XPS, the data we obtained can be correlated with surface modifications. Again, we have varied the flattening time from 0 s to 2 days as shown in Fig. 6a, b. The data reveals that initially almost all of the carbon present on the sample is sp^2-hybridized. This is of no surprise since the electrons of pristine graphene form sp^2-hybridized orbitals. With increasing flattening time, we observed a growing amount of sp^3-hybridized as well as C–O bound carbon, which we explain by additional adventitious carbon from the EVAC-foil as a result of the flattening step. Supplementary Figs. 4 and 5 show additional XPS data of flattened Gr/Cu. To estimate the amount of carbon residues on graphene after flattening, we compared the carbon signal originating from graphene to the overall carbon intensity, as presented in Fig. 6d for EVAC and various other materials. Despite the direct contact to the EVAC-foil, graphene still contributes 48% to the total C signal after being in contact with the foil for two days, which is a similar value when using other polymer-based materials or aluminum. Interestingly, similarly processed Gr/Cu samples flattened with a polycarbonate (PC) foil sometimes also allow successful transfers comparable to the EVAC-flattened samples. Notably, the XPS spectra of EVAC- and PC-flattened Gr/Cu are almost identical (Supplementary Fig. 6). Despite this, all other Gr/Cu samples flattened with, e.g., polyethylene terephthalate (PET), aluminum or simply old Gr/Cu sample not only show a signal of hydrophilic adsorbates, e.g., COOH groups, on graphene as presented for PET-flattened Gr/Cu in Fig. 6c, but also displayed the same ripping/crumbling behavior during the transfer as non-treated Gr/Cu.

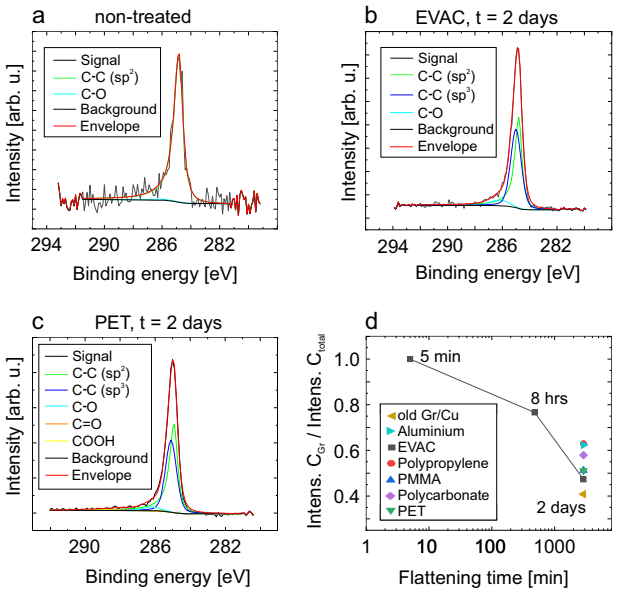

Fig. 6 XPS analysis of flattened graphene as well as evolution of sp^2- and sp^3- hybridized intensity ratio as a function of flattening time. XPS measurements of Gr/Cu samples that have been flattened before with various materials. **a**, **b** With increasing flattening time of the EVAC-foil additional carbon residues are deposited on graphene. **c** XPS spectrum of Gr/Cu after two days of flattening using a polyethylene terephthalate (PET) foil. **d** Intensity ratio of carbon signal originating from graphene compared to the total carbon signal for differently treated Gr/Cu samples as a function of time.

As a next step, we performed secondary ion-mass spectroscopy (ToF-SIMS) measurements to further understand the nature of the C-based material on graphene´s surface after having used EVAC for the flattening step. Figure 7 presents the results from this analysis. We observed a significant difference between treated and non-treated Gr/Cu for the mass of 59. After irradiating the Gr/Cu sample with Bi^{3+} ions and detecting the ejected material of the sample after ion impact, we observed negatively charged acetate groups being emitted from the surface, hence contributing with a total mass-charge ratio of 59 to this peak. While the flattened Gr/Cu sample shows a large signal at this particular mass compared to the signal in its close surrounding, the non-flattened sample shows no such striking feature. The presence of this peak at mass 59 for the flattened Gr/Cu sample can be linked directly to the flattening step, since the foil used for the flattening of the Gr/Cu shows the exact same signature, see Fig. 7b. Although, it is worth noting that during the flattening process no continuous polymer film of the foil is peeled off and attached to the graphene as we also observed EVAC-foil characteristic groups not being present on the flattened Gr/Cu. It is rather the presence of additional fragments of the EVAC foil including the characteristic acetate group which stick to graphene (Supplementary Fig. 7). With this observation, we can roughly estimate the coverage of these adsorbates. Since we could not observe any fingerprint of the acetate in the XPS measurements (e.g. a signal from C = O, which is present in the acetate) after using the EVAC-foil, but only witnessed their presence in the far more sensitive (ppb) ToF-SIMS measurements, we can deduce the density of the acetate groups to lie below 0.2 monolayer which corresponds to the sensitivity of the XPS.

A possible explanation for the increase of the mechanical stability after the EVAC-flattening step is based on lowering the difference in surface energy of graphene and the etching solution. If the difference in surface energy is small enough graphene would retain its shape allowing a successful transfer. In case of a large difference in surface energies between graphene and the etching solution, the system is expected to minimize its energy by reducing the surface area of graphene causing it to crumble. To test our hypothesis, we probed the contact angle of calibrated liquids with flattened and regular CVD graphene on copper. Generally, the interactions between a liquid and a solid depend on the chemical structure of the adsorbate and adsorbent and can be divided into polar and dispersive interactions. Polar interactions arise due to permanent or dipole-induced interactions, hence, strongly depend on the chemical structure of the investigated materials. Dispersive interactions on the contrary are caused by fluctuating electron densities and therefore are always present regardless of the chemical nature[40,41]. Both the polar σ^p and dispersive σ^d interactions contribute to the total surface energy σ of a liquid (subscript L) or solid (subscript S) and can be correlated according to the Owens–Wendt equation as:

$$\frac{\sigma_L(\cos\theta+1)}{2\sqrt{\sigma_L^d}} = \frac{\sqrt{\sigma_S^p}\sqrt{\sigma_L^p}}{\sqrt{\sigma_L^d}} + \sqrt{\sigma_S^d} \quad (1)$$

By probing the contact angles θ of well characterized test liquids with graphene, we are able to observe variations in both the polar and dispersive interactions. As shown in Fig. 8, the flattening step surprisingly does not increase but decreases the surface energy of the Gr/Cu surface from 40.6 mJ cm^{-2} to 37.8 mJ cm^{-2} for PET-flattened and 34.5 mJ cm^{-2} for EVAC-flattened Gr/Cu, respectively, meaning that the difference in surface energy with respect to water (σ_{water} ~72.8 mJ cm^{-2}) even increases. We

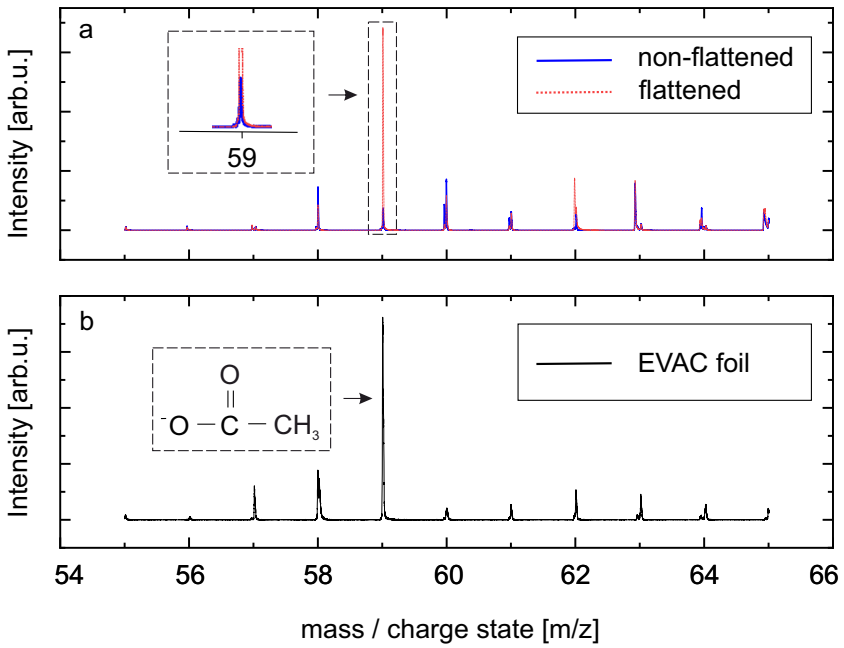

Fig. 7 ToF-SIMS analysis and surface modifications of regular and flattened Gr/Cu. ToF-SIMS measurement of **a** 1-day-flattened and non-flattened Gr/Cu and **b** bare EVAC-flattening foil. The data shows the negatively charged ion spectrum of the ToF-SIMS measurements.

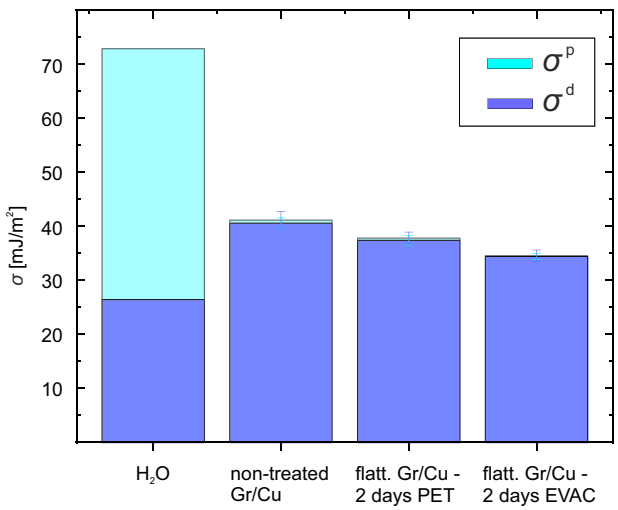

Fig. 8 Surface energy measurements of flattened and regular Gr/Cu. Polar and dispersive parts of surface energy of water, regular Gr/Cu, PET-, and EVAC-flattened Gr/Cu substrates. Error bars represent standard deviations.

can therefore rule out that it is the difference in surface tension, which causes the graphene to rip as often stated in literature[27,42,43]. Rather, we believe the reason for the increased mechanical stability during transfer to be due to the suppression of the polar interactions with the water molecules in the etching solution. While σ^d decreases by only 8% for PET-flattened and 14% for EVAC-flattened Gr/Cu, respectively, compared to non-treated samples, σ^p is reduced by 29% after PET- and 76% after EVAC-foil treatment. Considering that the polar part constitutes almost 2/3 of water's total surface energy, the flattening step seems to suppress the polar-polar interactions of the floating graphene sheet on the etching solution, hence preventing the graphene from tearing apart[44]. Supplementary Fig. 8 presents individual measurements of the contact angle for water, diiodmethane, and glycerol as test liquids.

In conclusion, we have developed a fast, inexpensive, and scalable way to increase the mechanical stability of graphene by flattening the Gr/Cu prior to the transfer using a regular EVAC-foil and a vacuum bag sealing machine. In addition to an extremely low-defect density and a considerably cleaner graphene surface due to the absence of any polymer support during the transfer, our technique may as well be used for intentional doping of graphene, as well as for increasing its hydrophobicity. We attribute the improvement of graphene´s properties in terms of mechanical stability during wet-chemical transfer to the suppression of polar-polar interaction.

METHODS

Flattening of Gr/Cu and sample preparation

Applying the flattening step of the Gr/Cu wafer using the ethylene-vinyl acetate copolymer foil is crucial for a successful polymer-free transfer. First, the Gr/Cu wafer (single-layer Gr/Cu from Graphenea, Spain) is placed onto a solid and smooth plate and covered by the ethylene-vinyl copolymer foil. The covered wafer including the plate are then placed into a regular plastic bag used for vacuum sealing. The vacuum sealing process presses the ethylene-vinyl acetate copolymer foil against the graphene (done with a regular commercially available vacuum bag sealing machine used for groceries, vegetables, etc.). The foil remains being pressed against the graphene for a minimum of 24 h. Afterwards, the Cu of the Gr/Cu wafer is etched off in an ammonium persulfate solution (7 g dissolved in 200 ml DI H_2O). The etching solution is diluted by DI water and the graphene can be scooped out with the target material.

Raman spectroscopy/AFM/XPS

Raman spectroscopy measurements have been performed using a Renishaw InVia Raman spectroscope with a 532 nm laser. In order to avoid heating effects, the laser power was kept below 100 µW.

AFM measurements were performed under ambient conditions with a Bruker Dimension FastScan microscope using the PeakForce Tapping mode.

XPS measurements were performed using the VersaProbe II microscope (UlvacPhi) with a monochromatic Al K-alpha source under a 45° angle with respect to the samples surface.

Contact-angle measurements

Contact angles were measured using a Contact-Angle System OCA 15EC (DataPhysics Instruments GmbH, Filderstadt, Germany). First, a 2 µl droplet was formed using an automatic dispenser unit. The sessile droplet was then formed by slowly approaching the substrate to the needle and removing it again after the droplet had contacted the samples surface. All test liquid measurements were carried out under ambient conditions.

ToF-SIMS measurements

ToF-SIMS data were obtained using an IONTOF ToF-SIMS 5 with a LMIG Bi^{3+} source operated at 30 kV. To avoid charging effects, we measured with a constantly running electron flood gun.

DATA AVAILABILITY

The datasets generated during and/or analyzed during the current study are available from the corresponding author on reasonable request. All data generated or analyzed during this study are included in this published article (and its Supplementary Information).

Received: 20 December 2019; Accepted: 10 April 2020;
Published online: 18 May 2020

REFERENCES

1. Geim, A. K. & Novoselov, S. The rise of graphene. *Nat. Mater.* **6**, 183–191 (2007).
2. Moving towards the market. *Nat. Mater.* **18**, 519 (2019).
3. Prydatko, A. V., Belyaeva, L. A., Jiang, L., Lima, L. M. C. & Schneider, G. F. Contact angle measurement of free-standing square-millimeter single-layer graphene. *Nat. Commun.* **9**, 4185 (2018).
4. Lin, L., Peng, H. & Liu, Z. Synthesis challenges for graphene industry. *Nat. Mater.* **18**, 520–524 (2019).
5. Liu, C. et al. Kinetic modulation of graphene growth by fluorine through spatially confined decomposition of metal fluorides. *Nat. Chem.* **11**, 730–736 (2019).
6. Nair, R. R., Wu, H. A., Jayaram, P. N., Grigorieva, I. V. & Geim, A. K. Unimpeded permeation of water through helium-leak-tight graphene-based membranes. *Science. (N. Y., N. Y.)* **335**, 442–444 (2012).
7. Yang, Q. et al. Ultrathin graphene-based membrane with precise molecular sieving and ultrafast solvent permeation. *Nat. Mater.* **16**, 1198–1202 (2017).
8. Seo, D. H. et al. Anti-fouling graphene-based membranes for effective water desalination. *Nat. Commun.* **9**, 683 (2018).
9. Zhou, K.-G. et al. Electrically controlled water permeation through graphene oxide membranes. *Nature* **559**, 236–240 (2018).
10. Madauß, L. et al. Fabrication of nanoporous graphene/polymer composite membranes. *Nanoscale* **9**, 10487–10493 (2017).
11. Wang, L. et al. Molecular valves for controlling gas phase transport made from discrete ångström-sized pores in graphene. *Nat. Nanotechnol.* **10**, 785–790 (2015).
12. Jain, T. et al. Heterogeneous sub-continuum ionic transport in statistically isolated graphene nanopores. *Nat. Nanotechnol.* **10**, 1053–1057 (2015).
13. Shin, S.-H. et al. Integrated arrays of air-dielectric graphene transistors as transparent active-matrix pressure sensors for wide pressure ranges. *Nat. Commun.* **8**, 14950 (2017).
14. Berger, C., Phillips, R., Centeno, A., Zurutuza, A. & Vijayaraghavan, A. Capacitive pressure sensing with suspended graphene-polymer heterostructure membranes. *Nanoscale* **9**, 17439–17449 (2017).
15. Zhu, Y., Cai, H., Ding, H., Pan, N. & Wang, X. Fabrication of low-cost and highly sensitive graphene-based pressure sensors by direct laser scribing polydimethylsiloxane. *ACS Appl. Mater. Interfaces* **11**, 6195–6200 (2019).
16. Mattevi, C., Kim, H. & Chhowalla, M. A review of chemical vapour deposition of graphene on copper. *J. Mater. Chem.* **21**, 3324–3334 (2011).
17. Reina, A. et al. Large area, few-layer graphene films on arbitrary substrates by chemical vapor deposition. *Nano Lett.* **9**, 30–35 (2009).
18. Chae, S. J. et al. Synthesis of large-area graphene layers on poly-nickel substrate by chemical vapor deposition: wrinkle formation. *Adv. Mater.* **21**, 2328–2333 (2009).
19. Kim, H. et al. Copper-vapor-assisted chemical vapor deposition for high-quality and metal-free single-layer graphene on amorphous SiO_2 substrate. *ACS Nano* **7**, 6575–6582 (2013).
20. Murdock, A. T. et al. Controlling the orientation, edge geometry, and thickness of chemical vapor deposition graphene. *ACS Nano* **7**, 1351–1359 (2013).
21. Xu, X. et al. Ultrafast epitaxial growth of metre-sized single-crystal graphene on industrial Cu foil. *Sci. Bull.* **62**, 1074–1080 (2017).
22. Bae, S. et al. Roll-to-roll production of 30-inch graphene films for transparent electrodes. *Nat. Nanotechnol.* **5**, 574–578 (2010).
23. Cherian, C. T. et al. 'Bubble-free' electrochemical delamination of CVD graphene films. *Small (Weinh. der Bergstr., Ger.)* **11**, 189–194 (2015).
24. Gao, L. et al. Face-to-face transfer of wafer-scale graphene films. *Nature* **505**, 190–194 (2014).
25. Kang, J., Shin, D., Bae, S. & Hong, B. H. Graphene transfer: key for applications. *Nanoscale* **4**, 5527–5537 (2012).
26. Kim, S. et al. Robust graphene wet transfer process through low molecular weight polymethylmethacrylate. *Carbon* **98**, 352–357 (2016).
27. Lin, W.-H. et al. A direct and polymer-free method for transferring graphene grown by chemical vapor deposition to any substrate. *ACS Nano* **8**, 1784–1791 (2014).
28. Kim, K. S. et al. Large-scale pattern growth of graphene films for stretchable transparent electrodes. *Nature* **457**, 706–710 (2009).
29. Li, X. et al. Transfer of large-area graphene films for high-performance transparent conductive electrodes. *Nano Lett.* **9**, 4359–4363 (2009).
30. van Ngoc, H., Qian, Y., Han, S. K. & Kang, D. J. PMMA-etching-free transfer of wafer-scale chemical vapor deposition two-dimensional atomic crystal by a water soluble polyvinyl alcohol polymer method. *Sci. Rep.* **6**, 33096 (2016).
31. Leong, W. S. et al. Paraffin-enabled graphene transfer. *Nat. Commun.* **10**, 867 (2019).
32. Gammelgaard, L. et al. Graphene transport properties upon exposure to PMMA processing and heat treatments. *2D Mater.* **1**, 35005 (2014).
33. Hallam, T., Berner, N. C., Yim, C. & Duesberg, G. S. Strain, bubbles, dirt, and folds: a study of graphene polymer-assisted transfer. *Adv. Mater. Interfaces* **1**, 1400115 (2014).
34. Choi, W., Shehzad, M. A., Park, S. & Seo, Y. Influence of removing PMMA residues on surface of CVD graphene using a contact-mode atomic force microscope. *RSC Adv.* **7**, 6943–6949 (2017).
35. Lin, Y.-C. et al. Graphene annealing: how clean can it be? *Nano Lett.* **12**, 414–419 (2012).
36. Johnson, B. Y., Mazumder, P. & Kamal Kishore. Johnson 2016 Graphene and polymer-free method for transferring cvd grown graphene onto hydrophobic substrates. Patent C01B 31/04, WO 2016/100418 A1 (2015).
37. Bruna, M. et al. Doping dependence of the Raman spectrum of defected graphene. *ACS Nano* **8**, 7432–7441 (2014).
38. Tripathi, M. et al. Cleaning graphene: comparing heat treatments in air and in vacuum. *Phys. Status Solidi RRL* **11**, 1700124 (2017).
39. Moser, J., Barreiro, A. & Bachtold, A. Current-induced cleaning of graphene. *Appl. Phys. Lett.* **91**, 163513 (2007).
40. Owens, D. K. Estimation of the surface free energy of polymers. *J. Appl. Polym. Sci.* **13**, 1741–1747 (1969).
41. Kisilev, A. V. Non-specific and specific interactions of molecules of different electronic structures with solid surfaces. *Discuss. Faraday Soc.* **40**, 205–218 (1965).
42. Zhang, G. et al. Versatile polymer-free graphene transfer method and applications. *ACS Appl. Mater. Interfaces* **8**, 8008–8016 (2016).
43. Park, H. et al. Polymer-free graphene transfer for enhanced reliability of graphene field-effect transistors. *2D Mater.* **3**, 21003 (2016).
44. Vargaftik, N. B., Volkov, B. N. & Voljak, L. D. International tables of the surface tension of water. *J. Phys. Chem. Ref. Data* **12**, 817–820 (1983).

ACKNOWLEDGEMENTS

We acknowledge support from the DFG by funding SCHL 384/16-1, ANR-15-GRFL-0002, and UL 113/10-1 (project number 279028710), and project C5 within the SFB1242 "Non-Equilibrium Dynamics of Condensed Matter in the Time Domain" (project number 278162697). R.J. greatly acknowledges the Alexander von *Humboldt Foundation Fellowship and Tobias Foller acknowledges the UNSW Scientia Ph.D scholarship. We also thank* Dr. Anne Rich und Dr. Chris Marjo from UNSW for fruitful discussions.

AUTHOR CONTRIBUTIONS

E.P., T.F., A.H., R.J., H.L., and A.B. contributed AFM, SEM. and FT-IR measurements to this work. ToF-SIMS measurements were performed and interpreted by T.H., M.H., L.S., and L.B. Contact-angle measurements were done and interpreted by J.S., A.W., and M. U. XPS measurements were performed and interpreted by U.H. L.M. and M.S. performed Raman measurements, developed the idea of this work, and wrote the manuscript.

COMPETING INTERESTS

The authors declare no competing interests.

ADDITIONAL INFORMATION

Supplementary information is available for this paper at https://doi.org/10.1038/s41699-020-0148-9.

Correspondence and requests for materials should be addressed to M.S.

Reprints and permission information is available at http://www.nature.com/reprints

Publisher's note Springer Nature remains neutral with regard to jurisdictional claims in published maps and institutional affiliations.